

Correlative piezoresponse and micro-Raman imaging of CuInP₂S₆–In_{4/3}P₂S₆ flakes unravels phase-specific phononic fingerprint via unsupervised learning F

Cite as: Appl. Phys. Lett. 121, 062901 (2022); <https://doi.org/10.1063/5.0101395>

Submitted: 31 May 2022 • Accepted: 15 July 2022 • Published Online: 08 August 2022

 M. Checa,  I. Ivanov,  S. M. Neumayer, et al.

COLLECTIONS

Note: This paper is part of the APL Special Collection on Phononics of Graphene, Layered Materials, and Heterostructures.

 This paper was selected as Featured



View Online



Export Citation



CrossMark

Lock-in Amplifiers
up to 600 MHz



Zurich
Instruments

Watch



Correlative piezoresponse and micro-Raman imaging of CuInP₂S₆–In_{4/3}P₂S₆ flakes unravels phase-specific phononic fingerprint via unsupervised learning



Cite as: Appl. Phys. Lett. **121**, 062901 (2022); doi: [10.1063/5.0101395](https://doi.org/10.1063/5.0101395)

Submitted: 31 May 2022 · Accepted: 15 July 2022 ·

Published Online: 8 August 2022



View Online



Export Citation



CrossMark

M. Checa,^{1,a)} I. Ivanov,¹ S. M. Neumayer,¹ M. A. Susner,² M. A. McGuire,³ P. Maksymovych,¹ and L. Collins¹

AFFILIATIONS

¹Center for Nanophase Materials Sciences, Oak Ridge National Laboratory, Oak Ridge, Tennessee 37831, USA

²Materials and Manufacturing Directorate, Air Force Research Laboratory, Wright-Patterson Air Force Base, Ohio 45433, USA

³Materials Science and Technology Division, Oak Ridge National Laboratory, Oak Ridge, Tennessee 37831, USA

Note: This paper is part of the APL Special Collection on Phononics of Graphene, Layered Materials, and Heterostructures.

^{a)}Author to whom correspondence should be addressed: checam@ornl.gov

ABSTRACT

Characterizing the novel properties of layered van der Waals materials is key for their application in functional devices. A better understanding of this type of material requires correlative imaging of diverse nanoscale material properties. Within this class of materials, CuInP₂S₆ (CIPS) has received a significant degree of interest due to its ionically mediated room temperature ferroelectricity. Moreover, it is possible to form stable self-assembled heterostructures of ferroelectric CuInP₂S₆ (CIPS) and non-ferroelectric (i.e., lacking Cu) In_{4/3}P₂S₆ (IPS) phases, by controlling the targeted composition and kinetics of synthesis. In this work, we present a correlative nanometric imaging study of the phononic modes and piezoelectricity of the phase-separated thin heteroepitaxial CIPS/IPS flakes. We show that it is possible to isolate the different phononic modes of the two phases by spatially correlating them with their distinct ferroelectric behavior. The coupling of our experimental data with unsupervised learning statistical methods enables unraveling specific Raman peaks that are characteristic of each chemical phase (CIPS and IPS) present in the composite sample, discarding the less significant ones.

Published under an exclusive license by AIP Publishing. <https://doi.org/10.1063/5.0101395>

van der Waals (vdW) layered ferroelectrics¹ are emerging as interesting material candidates for many applications due to the favorable interplay of their multiple functionalities involving ionic, phononic, electronic, optical, and thermal phenomena.^{1–3} Of particular interest, CuInP₂S₆ (CIPS) exhibits room temperature ferroelectricity and has gained much attention due to its promising applications in memristors,⁴ ion-gated synaptic transistors,⁵ electrochemical energy storage,² or neuromorphic computing.⁵ In addition, when synthesized with Cu deficiencies, a non-ferroelectric Cu-free phase (IPS) forms and increases the material's complexity and tunability. Due to the rich multifunctionality of vdW materials (in general) and CIPS/IPS composites (in particular), correlative microscopy is required to map the different properties in the same sample area on the micro- and nanoscale. Correlative microscopy consists of analyzing the same region of a sample with different microscopic imaging techniques to gain insight in the correlation between the different physicochemical properties measured by each technique individually.

In the case of CIPS, its polar behavior can be ionically mediated through the movement of the Cu atoms between the different stable positions beyond the unit cell and has previously been measured at the nanoscale by means of Piezoresponse Force Microscopy (PFM).^{6–12} PFM is the gold standard technique for characterization of minute electromechanical coupling with unmatched spatial resolution.¹³ The different atomic arrangement of the Cu and In ions (and vacancies) in the material crystallographic network leads to changes in its ferroelectricity and also determines the translational and rotational modes of the lattice. Spatially resolved micro-Raman spectroscopy (micro-RS)¹⁴ gives insight into such anion and cation phonon modes with sub-micrometric spatial resolution, by measuring a single Raman spectrum in a grid of points separated by hundreds of nanometers.

In this work, we present a correlative microscopy study of piezoelectric and phononic properties of the phase-separated thin heteroepitaxial CIPS/IPS flakes, which allows to identify the differences in phononic modes of the two phases by spatially correlating them with

their different electromechanical response. The deconvolution of the Raman fingerprints across the sample is aided by utilizing unsupervised machine learning clustering algorithms like principal component analysis (PCA) or k-means clustering, which allows us to more clearly identify phase-specific phononic responses.

The band excitation PFM (BE-PFM)¹⁵ used in this study combines a commercial Cypher AFM (Asylum Research, Santa Barbara, CA, USA) with a home-built LabVIEW software and National Instruments hardware to control the tip movement, data storage, and tip-sample excitation. We used Multi75E-G cantilevers with a conductive coating and a nominal spring constant of ~ 3 N/m and a free resonance frequency of ~ 75 kHz. We applied an ac voltage of 1 V amplitude over a band of frequencies centered around the contact resonance frequency of the cantilever.

In Fig. 1, we present the results applied to a ≈ 200 nm thick CIPS/IPS flake transferred onto a gold substrate by the scotch tape transfer method.¹⁶ Figures 1(a) and 1(b) show the optical and AFM topography images of the flake. A green dashed line following the flake's border is superimposed to all the images to guide the eye. The upper part of the flake shows a quite flat topography, whereas in the lower part of the flake a clearly distinguished topographical step allows us to have different thicknesses within the same flake. Figure 1(c) shows the (BE-PFM) amplitude of that flake at room temperature, where the previously mentioned heteroepitaxial CIPS/IPS phase separation is observed: the yellow/green areas exhibit an electromechanical response while the dark blue/purple areas are non-electromechanically responsive regions. We identify regions of finite piezoresponse as the ferroelectric CIPS regions and regions of zero piezoresponse as non-ferroelectric IPS regions (as well as the gold substrate). The power of BE-PFM is that the accurate tracking of the whole frequency response in every pixel avoids common PFM artifacts arising from frequency shifts due to different tip-sample contact stiffness or contrast related to

topographic changes. [We see that in Fig. 1(c) PFM is insensitive to the topographic steps of our flake.] Thus, combining optical, AFM and BE-PFM, we can separate structural and piezoresponse variation.

Micro-RS scans a laser ($\lambda = 785$ nm) over the sample in steps of 200 nm while collecting and measuring the energy of the inelastic scattered photons, after their interaction with the specimen's lattice. Even if micro-RS cannot compete with scanning probe microscopy (SPM) modes in terms of spatial resolution, we are going to show that it is accurate enough to visualize the CIPS/IPS phase separation¹⁷ (which usually is in the \sim hundreds of nm range). Thus, using correlative micro-RS and PFM, we can unravel the specific Raman fingerprint of the different phases, by allowing to identify the electromechanically active domains with the micro-RS spectra point by point, complementing previous reports, which tried a similar identification based on Bayesian linear unmixing¹⁸ of the local Raman signal. In addition, the relevance of our approach also comes from the fact that the phononic lattice vibrations of CIPS and IPS phases in the heteroepitaxial composite may differ from their responses measured in pure crystals as well as the well-known size effect^{7,19} of the distinct bulk response as compared to thin flakes.

Figures 1(d)–1(f) display the micro-RS maps corresponding to the peak intensity at 317, 375, and 558 cm^{-1} Raman shifts, respectively. Later, we will explain why we choose to show this specific Raman shifts here. We clearly observe that there is a good correlation between the CIPS/IPS phases from the BE-PFM image and the micro-RS maps (a couple of CIPS regions are highlighted with black and white dashed lines to guide the eye), indicating that the technique can differentiate the cation and anion phononic modes present in each individual chemical species.

Next, we implement PCA decomposition to the multidimensional micro-RS datasets to extract the corresponding eigenvalues and eigenvectors of most variance from our data (see Fig. 2). The first three

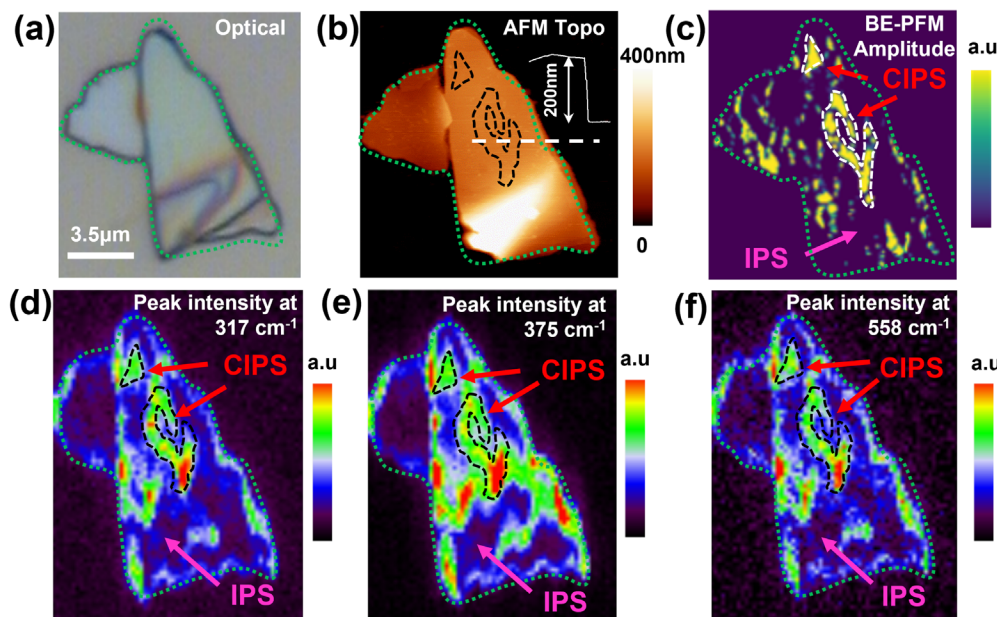


FIG. 1. Correlative PFM and micro-RS imaging. (a) Optical image of the CIPS/IPS flake. (b) AFM topography. (c) BE-PFM amplitude of the same flake. (d)–(f) Peak intensity map of the same flake at 317, 375, and 558 cm^{-1} Raman shifts correspondingly.

eigenvalue loading maps are shown in Figs. 2(a)–2(c). The corresponding eigenvectors are displayed in Fig. 2(d) and the scree plot of the first 10 components in Fig. 2(e). The first component clearly allows us to mask the gold substrate from the imaged flake, as we observe that the background gold substrate appears to be black, whereas the whole flake expresses higher eigenvalues (blueish). We can also note that the corresponding first eigenvector resembles the mean spectral response of the averaged mean Raman response of the whole flake [black dashed line superimposed in Fig. 2(d)]. The second component clearly highlights the CIPS ferroelectric phase, as such phase is clearly emphasized in the second loading map [white dashed lines to guide the eye to where the CIPS phase is found, see Fig. 1(c) for comparison]. Similarly, the third component represents the IPS non-ferroelectric phase as the CIPS domains in this case appear darker. The interpretation of the second and third eigenvectors, as it is usual in PCA, is not so straightforward. They emphasize the regions where CIPS and IPS chemical separation differs more from the mean flake response, i.e., a frequency shift (up-down peak) seems to be highlighted for the frequencies shown to correlate with PFM (375 and 558 cm^{-1}). Finally, the scree plot confirms that the first three components are enough to reconstruct the meaningful features of our dataset, as higher eigenvalues are irrelevant in terms of variance explained [Fig. 2(e)].

Next, we performed k-means clustering with $k=2$ as we expect the different chemical and structural properties of CIPS and IPS phases to manifest as two different Raman signatures in our flake. The k-means is done over the datapoints previously masked using the first PCA component loading map (which we have shown that it separates the flake from the substrate), to avoid clustering of the gold substrate. The spatial distribution of the two obtained clusters within the flat part of the flake shows a good agreement with the different phases of the material [Fig. 2(f)]. The red cluster is in good agreement with the CIPS while the green cluster represents

the IPS. The corresponding centroids of each cluster in the form of Raman spectra for each phase are shown in Fig. 2(g). Contrary to what happens with the PCA eigenvectors, k-means centroids are easier to interpret as they represent the mean response of each cluster instead of spectral directions of increased variance within our data. Hence, the centroid spectra show the main characteristic fingerprint of the previously studied^{20–22} Raman spectra of such metal thiophosphates (MTPs). The peaks found in the $200\text{--}350\text{ cm}^{-1}$ range correspond to distortions of the S-P-S bonds $\delta(\text{SPS})$. Particularly, the peak at 317 cm^{-1} is attributed to deformation of within the S_6 octahedron occupied by the Cu cation.²³ Therefore, as we will see in deep later, this peak is especially sensitive to the type of metal ion present in the lattice. The high intensity peak around the 375 cm^{-1} is attributed to P-P stretching $\nu(\text{PP})$, and the peaks appearing on the high frequency regime of the Raman shift are PS_3 stretching modes $\nu(\text{PS}_3)$. In the $\nu(\text{PS}_3)$ spectral region, the intensity peak at 558 cm^{-1} is again especially sensitive to the Cu ion presence. While all these vibrational modes are generally common to all the family of metal thio- and seleno-phosphates (MTPs),^{20,21} we can easily see by eye differences in the peak position, intensity, and width, in the $\delta(\text{SPS})$, $\nu(\text{PP})$, $\nu(\text{PS}_3)$ between the CIPS and IPS phases indicating possible local phononic differences induced by the presence of copper in the crystal lattice.

To get further insight on which of such peaks are more sensitive to the presence of CIPS, in Fig. 3, we show the Raman intensity maps at different peak locations along the spectra. First, we observe that for some Raman shifts: 254, 268, 298, and 564 cm^{-1} (labeled as “border” in red), even if the k-means centroid and PCA eigenvalues show differences there, the intensity maps do not correspond with the PFM phase separation. However, what we find is an enhancement of the Raman intensity at the borders of the flake, or at the flake steps, which suggest that either the Raman signal has a certain degree of convolution with the topography (probably due to either orientational, chemical, or

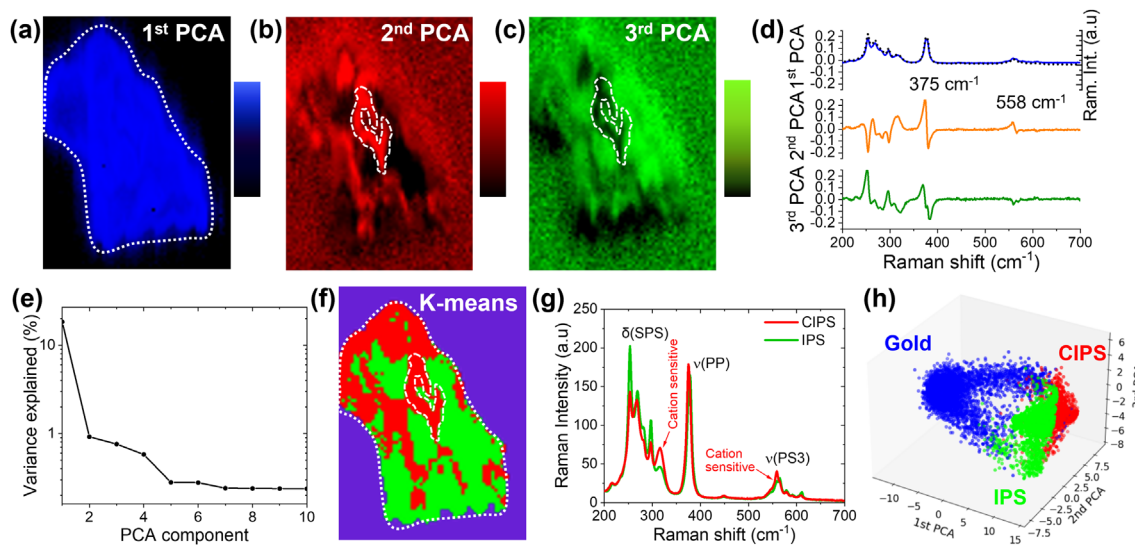


FIG. 2. PCA decomposition of micro-RS. Spatially resolved eigenvalue maps for the first three PCA components (a)–(c). Corresponding eigenvectors (d). Black dashed line is the superimposed averaged spectra of the whole flake. Scree plot is shown in (e). K-means clustering is shown in (f) with corresponding centroids in (g). Point cloud of the distribution of pixels along the first PCA components labeled by k-means color.

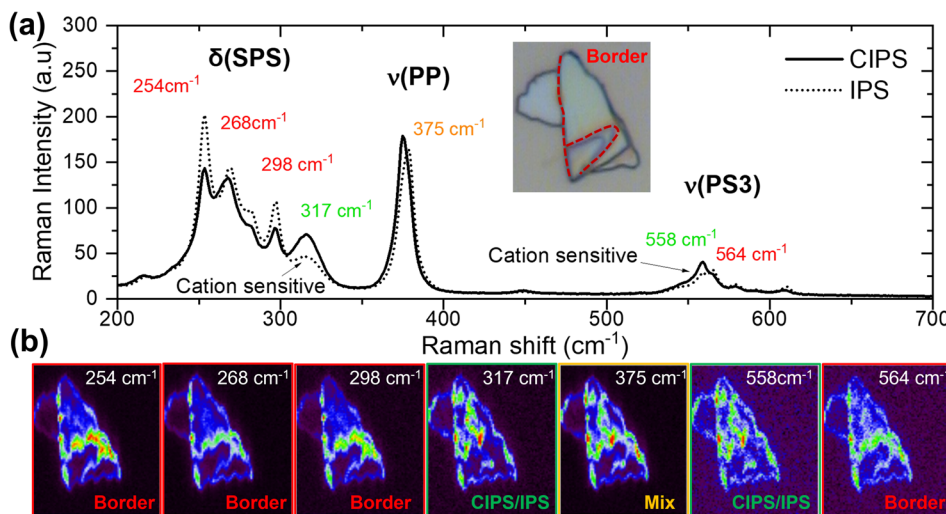


FIG. 3. (a) Raman spectra centroids of the k-means clustering separating CIPS and IPS contributions. (b) Images of intensity at certain frequency, separated between frequencies with signal enhanced at the topographical borders (red), at the CIPS/IPS domains (green), or at both mixed (orange).

electromagnetic Raman enhancement²⁴) or that the different penetration depth of the technique unravels a complex internal 3D phase structure. Next, for some other frequencies: 317 and 558 cm⁻¹, the clear one-to-one correlation with the PFM indicates that probably such peaks represent the most relevant phononic changes between CIPS and IPS. For the case of the peak at 317 cm⁻¹, the metallic cation presence and location within the S₆ octahedron modify the δ(SPS),²³ whereas the same happens with the stretching modes ν(PS₃) of the peak around 558 cm⁻¹.²⁵ Finally, there are other frequencies like 375 cm⁻¹ (labeled “mix” in orange), where both signals (border/topographic and CIPS/IPS separation) seem to be convoluted.

In conclusion, our findings permit identifying specific Raman peaks that are characteristic of each phase and separate them from the less relevant ones. As we have shown, one-to-one correlation with PFM spatial maps together with unsupervised learning methods is needed to unravel such information, as classical peak analysis of the Raman spectra alone is not enough to clarify which phononic modes are more characteristic of each chemical species. We expect that our results suggest ideas of how to manipulate lattice strain of CIPS/IPS composites and other related 2D vdW functional materials.

This work was supported by Center for Nanophase Materials Sciences (CNMS), which is a U.S. Department of Energy, Office of Science User Facility at Oak Ridge National Laboratory.

AUTHOR DECLARATIONS

Conflict of Interest

The authors have no conflicts to disclose.

Author Contributions

Martí Checa: Conceptualization (lead); Data curation (lead); Writing – original draft (lead). **Ilia N Ivanov:** Data curation (supporting); Writing – review and editing (supporting). **Sabine M Neumayer:** Investigation (supporting); Writing – review and editing (supporting). **Michael A. Susner:** Resources (supporting); Writing – review and editing (equal). **Michael A. McGuire:** Resources (supporting);

Writing – review and editing (supporting). **Petro Maksymovych:** Investigation (supporting); Writing – review and editing (supporting). **Liam Collins:** Supervision (lead); Writing – review and editing (lead).

DATA AVAILABILITY

The data that support the findings of this study are available from the corresponding author upon reasonable request.

REFERENCES

- ¹F. Xue, J.-H. He, and X. Zhang, “Emerging van der Waals ferroelectrics: Unique properties and novel devices,” *Appl. Phys. Rev.* **8**(2), 021316 (2021).
- ²M. A. Susner, M. Chyasnichiyus, M. A. McGuire, P. Ganesh, and P. Maksymovych, “Metal thio- and selenophosphates as multifunctional van der Waals layered materials,” *Adv. Mater.* **29**(38), 1602852 (2017).
- ³X.-Q. Yan, X. Zhao, H. Xu, L. Zhang, D. Liu, Y. Zhang, C. Huo, F. Liu, J. Xie, and X. Dong, “Temperature-tunable optical properties and carrier relaxation of CuInP₂S₆ crystals under ferroelectric-paraelectric phase transition,” *J. Mater. Chem. C* **10**(2), 696–706 (2022).
- ⁴X. Jiang, X. Wang, X. Wang, X. Zhang, R. Niu, J. Deng, S. Xu, Y. Lun, Y. Liu, and T. Xia, “Manipulation of current rectification in van der Waals ferroionic CuInP₂S₆,” *Nat. Commun.* **13**(1), 1–8 (2022).
- ⁵J. Chen, C. Zhu, G. Cao, H. Liu, R. Bian, J. Wang, C. Li, J. Chen, Q. Fu, and Q. Liu, “Mimicking neuroplasticity via ion migration in van der Waals layered copper indium thiophosphate,” *Adv. Mater.* **34**, 2104676 (2022).
- ⁶J. A. Brehm, S. M. Neumayer, L. Tao, A. O’Hara, M. Chyasnichiyus, M. A. Susner, M. A. McGuire, S. V. Kalinin, S. Jesse, and P. Ganesh, “Tunable quadruple-well ferroelectric van der Waals crystals,” *Nat. Mater.* **19**(1), 43–48 (2020).
- ⁷M. Chyasnichiyus, M. A. Susner, A. V. Ievlev, E. A. Eliseev, S. V. Kalinin, N. Balke, A. N. Morozovska, M. A. McGuire, and P. Maksymovych, “Size-effect in layered ferroelectric CuInP₂S₆,” *Appl. Phys. Lett.* **109**(17), 172901 (2016).
- ⁸M. Checa, S. Neumayer, M. A. Susner, M. A. McGuire, P. Maksymovych, and L. Collins, “Simultaneous mapping of nanoscale dielectric, electrochemical, and ferroelectric surface properties of van der Waals layered ferroelectric via advanced SPM,” *Appl. Phys. Lett.* **119**(25), 252905 (2021).
- ⁹S. M. Neumayer, Z. Zhao, A. O’Hara, M. A. McGuire, M. A. Susner, S. T. Pantelides, P. Maksymovych, and N. Balke, “Nanoscale control of polar surface phases in layered van der Waals CuInP₂S₆,” *ACS Nano* **16**, 2452 (2022).
- ¹⁰N. Balke, S. M. Neumayer, J. A. Brehm, M. A. Susner, B. J. Rodriguez, S. Jesse, S. V. Kalinin, S. T. Pantelides, M. A. McGuire, and P. Maksymovych, “Locally

- controlled Cu-ion transport in layered ferroelectric CuInP₂S₆,” *ACS Appl. Mater. Interfaces* **10**(32), 27188–27194 (2018).
- ¹¹S. M. Neumayer, J. A. Brehm, L. Tao, A. O’Hara, P. Ganesh, S. Jesse, M. A. Susner, M. A. McGuire, S. T. Pantelides, and P. Maksymovych, “Local strain and polarization mapping in ferrielectric materials,” *ACS Appl. Mater. Interfaces* **12**(34), 38546–38553 (2020).
- ¹²M. A. Susner, A. Belianinov, A. Borisevich, Q. He, M. Chyasanavichyus, H. Demir, D. S. Sholl, P. Ganesh, D. L. Abernathy, and M. A. McGuire, “High- T_c layered ferrielectric crystals by coherent spinodal decomposition,” *ACS Nano* **9**(12), 12365–12373 (2015).
- ¹³A. Gruverman and S. V. Kalinin, “Piezoresponse force microscopy and recent advances in nanoscale studies of ferroelectrics,” *J. Mater. Sci.* **41**(1), 107–116 (2006).
- ¹⁴D. Graf, F. Molitor, K. Ensslin, C. Stampfer, A. Jungen, C. Hierold, and L. Wirtz, “Spatially resolved Raman spectroscopy of single-and few-layer graphene,” *Nano Lett.* **7**(2), 238–242 (2007).
- ¹⁵S. Jesse, R. Vasudevan, L. Collins, E. Strelcov, M. B. Okatan, A. Belianinov, A. P. Baddorf, R. Proksch, and S. V. Kalinin, “Band excitation in scanning probe microscopy: Recognition and functional imaging,” *Annu. Rev. Phys. Chem.* **65**, 519–536 (2014).
- ¹⁶K. S. Novoselov, A. K. Geim, S. V. Morozov, D.-E. Jiang, Y. Zhang, S. V. Dubonos, I. V. Grigorieva, and A. A. Firsov, “Electric field effect in atomically thin carbon films,” *Science* **306**(5696), 666–669 (2004).
- ¹⁷A. Belianinov, Q. He, A. Dziaugys, P. Maksymovych, E. Eliseev, A. Borisevich, A. Morozovska, J. Banys, Y. Vysochanskii, and S. V. Kalinin, “CuInP₂S₆ room temperature layered ferroelectric,” *Nano Lett.* **15**(6), 3808–3814 (2015).
- ¹⁸A. V. Ievlev, M. A. Susner, M. A. McGuire, P. Maksymovych, and S. V. Kalinin, “Quantitative analysis of the local phase transitions induced by laser heating,” *ACS Nano* **9**(12), 12442–12450 (2015).
- ¹⁹L. Chen, Y. Li, C. Li, H. Wang, Z. Han, H. Ma, G. Yuan, L. Lin, Z. Yan, and X. Jiang, “Thickness dependence of domain size in 2D ferroelectric CuInP₂S₆ nanoflakes,” *AIP Adv.* **9**(11), 115211 (2019).
- ²⁰R. Rao, B. S. Conner, R. Selhorst, and M. A. Susner, “Pressure-driven phase transformations and phase segregation in ferrielectric CuInP₂S₆–In_{4/3}P₂S₆ self-assembled heterostructures,” *Phys. Rev. B* **104**(23), 235421 (2021).
- ²¹R. Rao, R. Selhorst, B. S. Conner, and M. A. Susner, “Ferrielectric-paraelectric phase transitions in layered CuInP₂S₆ and CuInP₂S₆–In_{4/3}P₂S₆ heterostructures: A Raman spectroscopy and x-ray diffraction study,” *arXiv:2111.00615* (2021).
- ²²S. N. Neal, S. Singh, X. Fang, C. Won, F.-T. Huang, S.-W. Cheong, K. M. Rabe, D. Vanderbilt, and J. L. Musfeldt, “Vibrational properties of CuInP₂S₆ across the ferroelectric transition,” *Phys. Rev. B* **105**(7), 075151 (2022).
- ²³Y. M. Vysochanskii, V. Stephanovich, A. Molnar, V. Cajipe, and X. Bourdon, “Raman spectroscopy study of the ferrielectric-paraelectric transition in layered CuInP₂S₆,” *Phys. Rev. B* **58**(14), 9119 (1998).
- ²⁴S. Kumar, K. Tokunaga, K. Namura, T. Fukuoka, and M. Suzuki, “Experimental evidence of a twofold electromagnetic enhancement mechanism of surface-enhanced Raman scattering,” *J. Phys. Chem. C* **124**(38), 21215–21222 (2020).
- ²⁵Y. Mathey, R. Cle, J. Audiere, O. Poizat, and C. Sourisseau, “Structural, vibrational and conduction properties of a new class of layer-type MPS₃ compounds: Mn^{II}_{1-x}M^I_xPS₃ (M^I = Cu, Ag),” *Solid State Ion.* **9–10**, 459–465 (1983).